IEEE Access
Multidisciplinary | Rapid Review | Open Access Journal

Received December 12, 2017, accepted January 6, 2018, date of publication January 11, 2018, date of current version February 28, 2018.

Digital Object Identifier 10.1109/ACCESS.2018.2791991

Designs of Diplexing Power Dividers

PU-HUA DENG, (Member, IEEE), WEI LO, BO-LIN CHEN, AND CHEN-HSIANG LIN
Department of Electrical Engineering, National University of Kaohsiung, Kaohsiung 811, Taiwan

Corresponding author: Pu-Hua Deng (phdeng@nuk.edu.tw)

This work was supported by the Ministry of Science and Technology (MOST), Taiwan, under Grant MOST 104-2221-E-390-007 and Grant MOST 105-2221-E-390-003.

ABSTRACT A diplexer with different-frequency power dividers cascaded to its output ports can split a signal into different frequency bands for power dividing functions. However, the design of a diplexer usually requires two different frequency filters. This paper presents three new microstrip diplexing power dividers (DPDs) to achieve duplexing power division without requiring additional filters. Moreover, to increase selectivity, each of the proposed DPDs has the flexibility of adding a dual-band filter to its input port. In particular, the proposed DPDs have matching circuits integrated in the dividers, enabling each divider with imaginary input impedance to reach the required open condition; this is achieved by designing a 50-Ω transmission line of appropriate length or a quarter-wavelength (λ/4) transmission line.

INDEX TERMS Diplexing, divider, matching circuit, quarter wavelength, Wilkinson.

I. INTRODUCTION

The main function of a diplexer is to transfer different band signals to the corresponding channels. Planar diplexers have been widely investigated for wireless front-end circuits [1]–[12]. For example, [1]–[10] reported on the bandpass response in each channel diplexers. In addition, [11] and [12] have presented low-pass-bandpass diplexers, and [2]–[5] and [7] have improved the selectivity and isolation of diplexers. Moreover, [3]–[8] and [10] have proposed diplexers for compact and ultra-wideband applications, and [9] proposed a diplexer with edge-coupled filters to avoid the size of matching circuit. However, in [9], external quality factor realization for non-narrowband filter response was difficult because of the limitation of coupled line distance.

Wilkinson power divider (WPD) [13] can be used for splitting power along different paths because of its simple design, low transmission loss, and high isolation properties. Several modified Wilkinson power dividers (WPDs) have been proposed for various requirements [14]–[24]. For example, [14], [15], [17], and [19] have presented compact WPDs; [16], [17], and [19] have focused on improving spurious responses. Recently, multiband and filtering dividers have received increasing research attention [18], [20]–[24].

In a dual-band front-end system, to transmit different frequency signals in different paths, each path requires the power to be split along two transmission channels. Intuitively, a circuit can be designed by cascading WPDs with different frequency bands to the output ports of a diplexer. However, this usually requires the use of different band filters in diplexers, as in [2]–[4] and [7]. Therefore, this paper proposes three new microstrip diplexing power divider (DPD) circuits, denoted as DPD 1, DPD 2, and DPD 3. The three DPDs were used as power dividers to design diplexing circuits. Compared with a diplexer cascaded to a divider at each of its output ports, the proposed DPDs without filters can separate signals for transmission through different frequency band channel dividers. The selectivity can be improved by incorporating a dual-band bandpass filter, as in [25] or [26], at the input ports of each proposed DPD.

Integration of matching circuits in each of the proposed DPDs is an important design step because it avoids the unwanted loading effect. In DPD 1, shunt open stub is designed at each divider transmission paths to produce short circuits such that each divider has pure imaginary input impedance at the unwanted loading channel operating frequency. Therefore, the required open condition of the unwanted loading channel can be easily achieved by adding a 50-Ω transmission line of appropriate length at each divider input. At unwanted loading channel operating frequency, DPD 2 or DPD 3 uses a shunt open stub at each divider input to produce a short circuit at the divider input; the open condition can be achieved by adding a quarter-wavelength (λ/4) transmission line before each divider input. The matching concept of DPD 2 or DPD 3 using a λ/4 line before an equivalent short circuit to meet the open condition is similar to that in [12] and [26]. To the best of our knowledge, the use

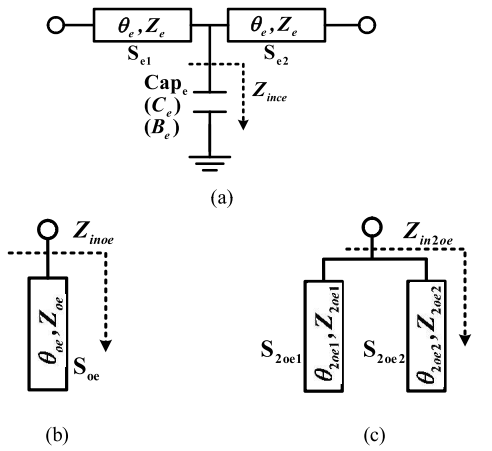

FIGURE 1. Equivalent circuit of a T-shaped transformer and two shunt capacitance equivalent circuits. (a) T-shaped transformer. (b) Shunt open stub. (c) Two shunt open stubs.

of power dividers for different frequency bands to design diplexing circuits has not yet been reported in the literature.

II. DESIGN OF DPD 1

Fig. 1(a) shows a T-shaped impedance transformer such as that in [17]; this transformer has two series transmission lines, S_{e1} and S_{e2} (all parameters of the two lines are the same), and one shunt capacitor with C_e capacitance. The characteristic impedance and electrical length of S_{e1} or S_{e2} are Z_e and θ_e, respectively. The design equation for each $\lambda/4$ impedance transformer of conventional WPD and the T-shaped impedance transformer in Fig. 1(a) can be written as

$$B_e Z_e^2 = \left(\frac{Z_e^2}{Z_1} - Z_1\right) \tag{1}$$

$$0 = \cos 2\theta_e - \frac{1}{2} Z_e B_e \sin 2\theta_e \tag{2}$$

where B_e is susceptance of C_e and Z_1 is the characteristic impedance of WPD transformer. The T-shaped impedance transformer is used to design the proposed DPD 1. DPD 1 has low- and high-band power dividers with center frequencies f_1 and f_2, respectively, where $f_2 > f_1$. Figs. 1(b) and 1(c) show two possible structures to implement the capacitance of Fig. 1(a). The T-shaped impedance transformer plays two important roles: The first role is to replace $\lambda/4$ impedance transformers of the conventional WPD, and the second is to provide a short circuit for the matching condition, where C_e can be designed using structures such as those illustrated in Figs. 1(b) and 1(c).

In general, the capacitance C_e of the T-shaped impedance transformer in Fig. 1(a) is not large considering the realizable range of microstrip line section S_{e1}/S_{e2}. Therefore, using only the one open stub of Fig. 1(b) to design $\lambda/4$ at f_2 for designing a short circuit at f_2 and to fit the small capacitance C_e at f_1 is difficult for a low-band divider when the ratio of f_2 to f_1 is not large, i.e., the open stub length

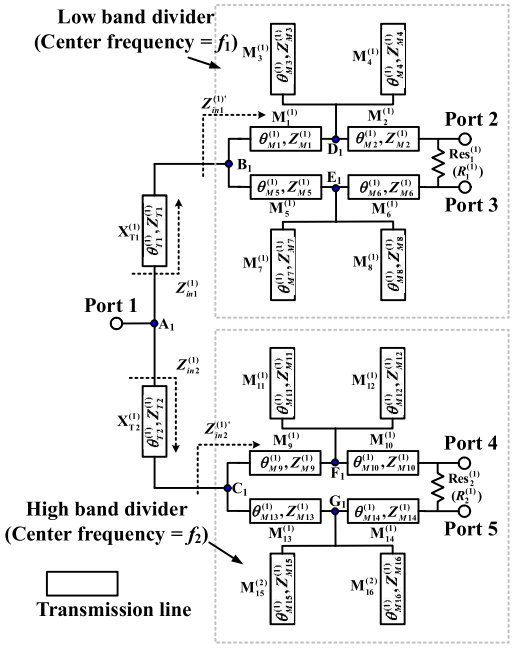

FIGURE 2. Equivalent circuit of proposed DPD 1.

of $\lambda/4$ at f_2 is not short. Similarly, in a high-band divider, C_e in the T-shaped impedance transformer of Fig. 1(a) is often unsuitable for using only one open stub to design a short circuit for the low-band matching condition and achieve the required capacitance at the same time. To overcome the issue of using only one open stub, capacitance C_e of the T-shaped transformer in Fig. 1(a) can be realized by using two shunt open stubs of Fig. 1(c). If capacitance C_e of the T-shaped transformer in Fig. 1(a) is designed using two open stubs of Fig. 1(c) for a low-band divider, the electrical length of open stub S_{2oe1} is 90° at $f_2(\theta_{2oe1}\big|_{f=f_2} = 90°)$, which can provide a short circuit for the high-band matching condition. Because $f_2 > f_1$, $\theta_{2oe1}\big|_{f=f_1} < 90°$; that is, the open stub S_{2oe1} can be equivalent to a parallel capacitance or a positive susceptance at f_1. The susceptance of the open stub S_{2oe1} can be increased by appropriately designing the susceptance of open stub S_{2oe2} under a fixed required equivalent susceptance of C_e. By increasing the susceptance of the open stub S_{2oe1}, the characteristic impedance of S_{2oe1} can be decreased. That is, the high characteristic impedance (difficult realization in microstrip form) when using only a single open stub S_{oe} of Fig. 1(b) can be effectively relaxed. In other words, S_{2oe1} and S_{2oe2} can be easily realized in microstrip form under reasonable Z_{2oe1} and Z_{2oe2}values. Similarly, S_{2oe1} and S_{2oe2} can also be easily realized in microstrip form in high-band divider under reasonable Z_{2oe1} and Z_{2oe2} values for low-band short matching circuit and high band required capacitance.

Fig. 2 illustrates the equivalent circuit of the proposed DPD 1 comprising a low-band divider, a high-band divider, and two matching lines ($X_{T1}^{(1)}$ and $X_{T2}^{(1)}$) with Z_0 ($Z_0 = 50\ \Omega$ system impedance) characteristic impedance, wherein the WPD is used as the low/high-band divider by replacing the T-shaped

equivalent transformer of Fig. 1(a) with each λ/4 impedance transformer. Therefore, the resistance $R_1^{(1)}$ or $R_2^{(1)}$ is $2Z_0$. The center frequencies of the low-band divider and high-band divider are f_1 and f_2, respectively. The low-band divider has a horizontal symmetry. The top-half transmission line circuit comprising $M_1^{(1)}$, $M_2^{(1)}$, $M_3^{(1)}$, and $M_4^{(1)}$ is equivalent to the T-shaped transformer in Fig. 1(a), wherein the capacitance C_e is realized by using two shunt open stubs of Fig. 1(c). The transmission line parameters of $M_1^{(1)}/M_2^{(1)}$ equal those of S_{e1}/S_{e2}. The sum susceptance of open stubs $M_3^{(1)}$ and $M_4^{(1)}$ equals that of C_e in Fig. 1(a). The open stub $M_3^{(1)}$ is λ/4 at f_2. In other words, Point D_1/E_1 is a short circuit at f_2. Therefore, the behavior in the direction from Point B_1 to Port 2/Port 3 can be equivalent to when using two short stubs $M_1^{(1)}$ and $M_5^{(1)}$ in parallel, that is, the input impedance $Z_{in1}^{(1)'}|_{f=f_2}$ at Point B_1 is a purely imaginary number. The input impedance $Z_{in1}^{(1)}|_{f=f_2}$ can reach infinity by adjusting the length of the matching line $X_{T1}^{(1)}$ of Z_0. On the basis of this design, the loading effect from the low-band circuit to the high-band circuit can be ignored.

The high-band divider has horizontal symmetry, with a design similar to that of the low-band divider. The required capacitance C_e of each path can be realized by using two shunt open stubs of Fig. 1(c) and the input impedance $Z_{in2}^{(1)}|_{f=f_1}$ can reach infinity by adjusting the length of the matching line $X_{T2}^{(1)}$ of Z_0.

The two band center frequencies of DPD 1 are $f_1 = 1.8$ GHz and $f_2 = 2.4$ GHz. On the basis of the aforementioned design in this section, the electrical length of $M_3^{(1)}$ at f_2 is $\theta_{M3}^{(1)}|_{f=f_2} = 90°$ or at f_1 is $\theta_{M3}^{(1)}|_{f=f_1} = 67.5° < 90°$. The open stub $M_3^{(1)}$ at f_1 is equivalent to a capacitor in parallel. Open stubs $M_4^{(1)}$ and $M_8^{(1)}$ shunt to $M_3^{(1)}$ and $M_7^{(1)}$, respectively, where the electrical length of $M_4^{(1)}/M_8^{(1)}$ at f_1 is $135° > \theta_{M4}^{(1)}|_{f=f_1} > 90°/135° > \theta_{M8}^{(1)}|_{f=f_1} > 90°$, that is, the open stub $M_4^{(1)}/M_8^{(1)}$ at f_1 is equivalent to an inductor in parallel. Therefore, the open stub $M_3^{(1)}/M_7^{(1)}$ and open stub $M_4^{(1)}/M_8^{(1)}$ at f_1 are equivalent to positive susceptance and negative susceptance, respectively. The susceptance of the open stub $M_3^{(1)}/M_7^{(1)}$ can increase by appropriately designing the susceptance of open stub $M_4^{(1)}/M_8^{(1)}$ under a fixed required equivalent susceptance of C_e. By increasing the susceptance of the open stub $M_3^{(1)}/M_7^{(1)}$, the characteristic impedance of $M_3^{(1)}/M_7^{(1)}$ can be decreased. In other words, the high characteristic impedance (difficult realization in microstrip form) when using only single $M_3^{(1)}/M_7^{(1)}$ without $M_4^{(1)}/M_8^{(1)}$ in parallel can be effectively relaxed. The design parameters of the low-band channel circuit are $R_1^{(1)} = 100\ \Omega$, $\theta_{M1}^{(1)}|_{f=f_1} = \theta_{M2}^{(1)}|_{f=f_1} = 37.71°$, $\theta_{M5}^{(1)}|_{f=f_1} = \theta_{M6}^{(1)}|_{f=f_1} = 37.71°$, $\theta_{M3}^{(1)}|_{f=f_1} = \theta_{M7}^{(1)}|_{f=f_1} = 67.5°$ or $\theta_{M3}^{(1)}|_{f=f_2} = \theta_{M7}^{(1)}|_{f=f_2} = 90°$, $\theta_{M4}^{(1)}|_{f=f_1} = \theta_{M8}^{(1)}|_{f=f_1} = 120°$, $Z_{M1}^{(1)} = Z_{M2}^{(1)} = Z_{M3}^{(1)} = Z_{M5}^{(1)} = Z_{M6}^{(1)} = Z_{M7}^{(1)} = 91.45\ \Omega$, and $Z_{M4}^{(1)} = Z_{M8}^{(1)} = 83.67\ \Omega$, where $\theta_{Mk}^{(1)}(k = 1$ to $8)$ and $Z_{Mk}^{(1)}(k = 1$ to $8)$ are the electrical length and characteristic impedance, respectively. The electrical length $\theta_{M4}^{(1)}/\theta_{M8}^{(1)}$ is 120° at 1.8 GHz; that is, $\theta_{M4}^{(1)}/\theta_{M8}^{(1)}$ equals 90° at $f_{TZ1}^{(1)} = 1.35$ GHz. Thus, the low-band divider of DPD 1 has a transmission zero at 1.35 GHz in each transmission path. The characteristic impedance and electrical length of $X_{T1}^{(1)}$ are $Z_{T1}^{(1)} = Z_0 = 50\ \Omega$ and $\theta_{T1}^{(1)} = 31.76°$ at $f_1 = 1.8$ GHz.

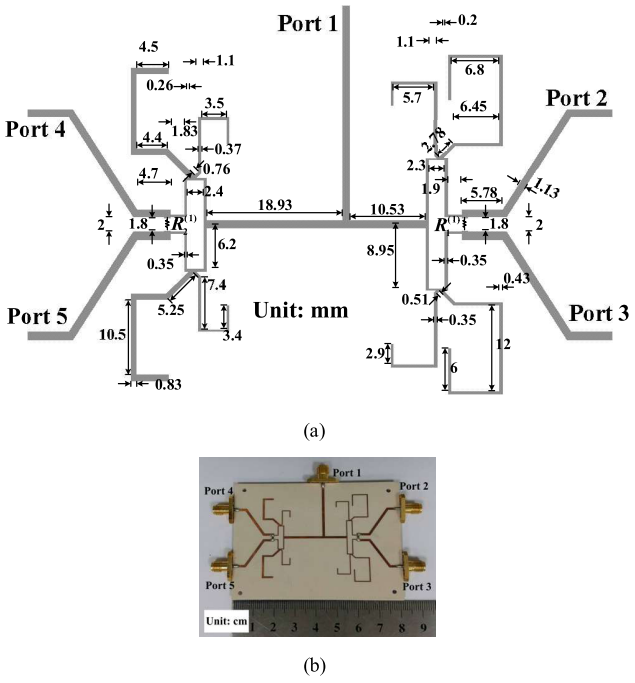

FIGURE 3. Proposed DPD 1 (a) layout and (b) photograph.

By the similar design concept of low-band channel, the high-band channel circuit can achieve the required matching and transmission conditions. The design parameters of the high-band channel circuit are $R_2^{(1)} = 100\ \Omega$, $\theta_{M9}^{(1)}|_{f=f_2} = \theta_{M10}^{(1)}|_{f=f_2} = 37.71°$, $\theta_{M13}^{(1)}|_{f=f_2} = \theta_{M14}^{(1)}|_{f=f_2} = 37.71°$, $\theta_{M11}^{(1)}|_{f=f_2} = \theta_{M15}^{(1)}|_{f=f_2} = 120°$ or $\theta_{M11}^{(1)}|_{f=f_1} = \theta_{M15}^{(1)}|_{f=f_1} = 90°$, $\theta_{M12}^{(1)}|_{f=f_2} = \theta_{M16}^{(1)}|_{f=f_2} = 72°$ or $\theta_{M12}^{(1)} = \theta_{M16}^{(1)} = 90°$ at $f_{TZ2}^{(1)} = 3$ GHz, $Z_{M9}^{(1)} = Z_{M10}^{(1)} = Z_{M13}^{(1)} = Z_{M14}^{(1)} = 91.45\ \Omega$, $Z_{M11}^{(1)} = Z_{M15}^{(1)} = 60\ \Omega$, and $Z_{M12}^{(1)} = Z_{M16}^{(1)} = 89\ \Omega$, where $\theta_{Mk}^{(1)}(k = 9$ to $16)$ and $Z_{Mk}^{(1)}(k = 9$ to $16)$ are the electrical length and characteristic impedance, respectively. The characteristic impedance and electrical length of $X_{T2}^{(1)}$ are $Z_{T2}^{(1)} = Z_0 = 50\ \Omega$ and $\theta_{T2}^{(1)} = 85.3°$ at $f_2 = 2.4$ GHz. Because $\theta_{M12}^{(1)} = \theta_{M16}^{(1)} = 90°$ at $f_{TZ2}^{(1)} = 3$ GHz and $\theta_{M11}^{(1)}|_{f=f_1} = 90°/\theta_{M15}^{(1)}|_{f=f_1} = 90°$, two transmission zeros for each path can be obtained at f_1 and $f_{TZ2}^{(1)}$, respectively.

In this study, an RO4003C substrate (thickness = 0.508 mm, dielectric constant = 3.65, and loss tangent = 0.0065) was used to fabricate all circuits. Fig. 3 demonstrates the circuit layout and photograph of the proposed DPD 1, wherein chip resistors are used to implement $R_1^{(1)}$ and $R_2^{(1)}$

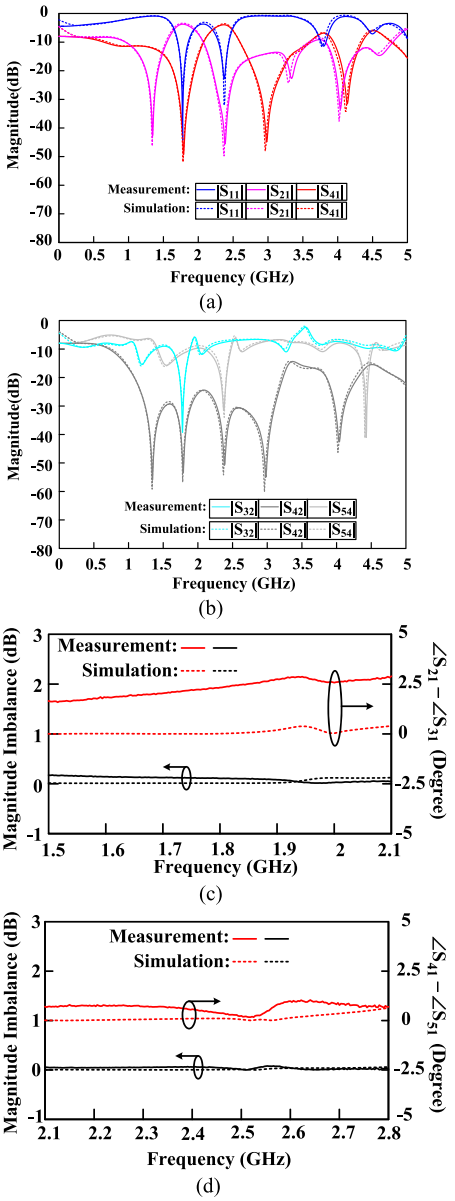

FIGURE 4. Measured and simulated responses of DPD 1. (a) $|S_{11}|$, $|S_{21}|$, and $|S_{41}|$. (b) $|S_{32}|$, $|S_{42}|$, and $|S_{54}|$. (c) Phase and magnitude imbalances of $|S_{21}|$ and $|S_{31}|$. (d) Phase and magnitude imbalances of $|S_{41}|$ and $|S_{51}|$.

in Fig. 2. Fig. 4 illustrates the simulated and measured frequency results of DPD 1. The measured minimal insertion loss ($-20\log|S_{21}|$) of the low-band divider was approximately 3.74 dB at 1.77 GHz, whereas that ($-20\log|S_{41}|$) of the high-band divider was approximately 3.95 dB at 2.38 GHz. The measured $|S_{42}|$ between two operating bands was less than −24 dB. The measured maximal isolations $-20\log|S_{32}|$ and $-20\log|S_{54}|$ of the low-band and high-band dividers were approximately 39 dB at 1.78 GHz and 31 dB at 2.375 GHz, respectively. The measured magnitude and phase imbalances of the low-band divider operating band were approximately 0–0.173 dB and 1.66°–2.89°, respectively. The measured magnitude and phase imbalances of high-band

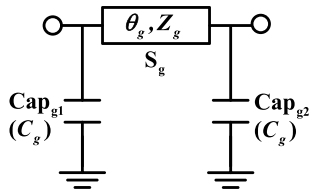

FIGURE 5. π-shaped impedance transformer with a series transmission line and two shunt capacitors.

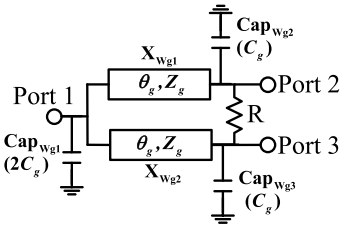

FIGURE 6. Modified WPD with a series transmission line and shunt capacitors in each transmission path.

divider operating band were approximately 0–0.08 dB and 0.175°–1.04°, respectively. For $|S_{42}|$, four transmission zeros were measured at approximately 1.344 GHz, 1.791 GHz, 2.381 GHz, and 2.984 GHz approaching specifications of $f_{TZ1}^{(1)}$, f_1, f_2, and $f_{TZ2}^{(1)}$, respectively; these are contributed by stubs $M_4^{(1)}$, $M_{11}^{(1)}$, $M_3^{(1)}$, and $M_{12}^{(1)}$, respectively. In addition, for $|S_{21}|$, two transmission zeros were measured at approximately 1.344 GHz and 2.388 GHz approaching specifications of $f_{TZ1}^{(1)}$ and f_2, respectively; these are contributed by $M_4^{(1)}$ and $M_3^{(1)}$, respectively. For S_{41}, two transmission zeros were measured at approximately 1.788 GHz and 2.981 GHz approaching specifications of f_1 and $f_{TZ2}^{(1)}$, respectively; these are contributed by stubs $M_{11}^{(1)}$ and $M_{12}^{(1)}$, respectively. The low/high-band dividers exhibit a bandpass filtering response with lower and higher stopband transmission zeros. Therefore, the stubs in DPD 1 can be used for matching, stopband suppression, and improving isolation roles.

III. DESIGN OF DPD 2

Fig. 5 illustrates a π-shaped impedance transformer having a series transmission line S_g with electrical length θ_g and characteristic impedance Z_g, and two shunt capacitors Cap_{g1} and Cap_{g2} with the same C_g capacitance. The design equations between the λ/4 impedance transformer of WPD and the π-shaped impedance transformer in Fig. 5 can be written as

$$Z_1 = Z_g \sin\theta_g \tag{3}$$

$$0 = \cos\theta_g - Z_g B_g \sin\theta_g \tag{4}$$

where B_g is the susceptance of C_g. A modified WPD [15] (Fig. 6) can be formed using the π-shaped impedance transformer to replace each λ/4 impedance transformer of the conventional WPD (Fig. 3). In Fig. 6, the capacitance of Cap_{wg1} is equivalent to two C_g in parallel, that is, the capacitance of Cap_{wg1} is $2C_g$. Fig. 7 presents the ideal equivalent

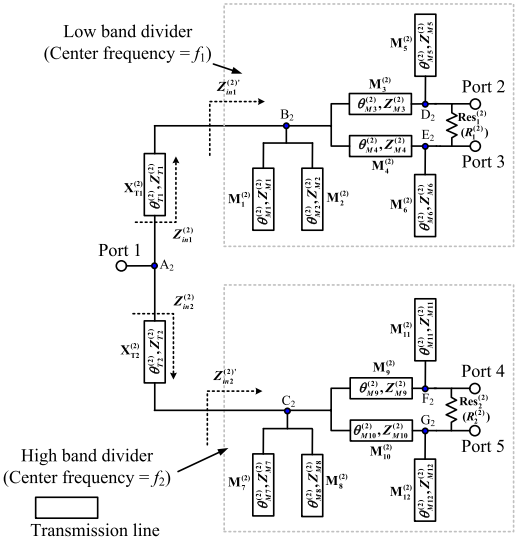

FIGURE 7. Equivalent circuit of the proposed DPD 2.

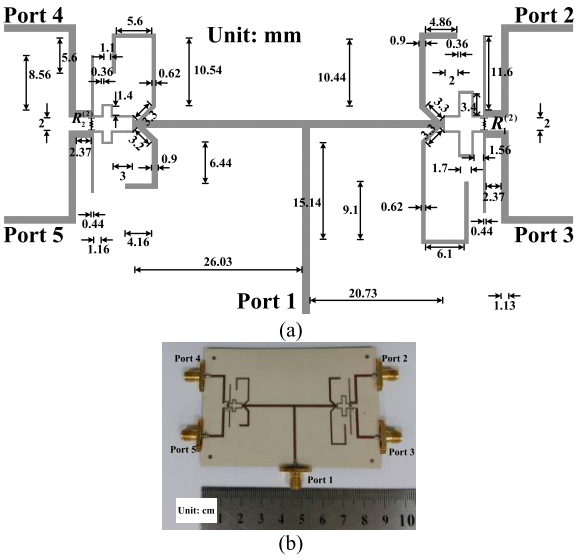

FIGURE 8. Proposed DPD 2 (a) layout and (b) photograph.

circuit of the proposed DPD 2 that comprises a low-band divider, a high-band divider, and two matching lines ($X_{T1}^{(2)}$ and $X_{T2}^{(2)}$) with Z_0 characteristic impedance, wherein the low/high-band divider equivalent circuit uses the modified WPD shown in Fig. 6. Therefore, the resistance $R_1^{(2)}$ or $R_2^{(2)}$ is $2Z_0$. The center frequencies of the low-band and high-band dividers are f_1 and f_2, respectively. The sum susceptance of open stubs $M_1^{(2)}$ and $M_2^{(2)}$ equals that of $2C_g$ in Fig. 6, wherein the use of the parallel stubs $M_1^{(2)}$ and $M_2^{(2)}$ is similar to that of parallel stubs $M_3^{(1)}$ and $M_4^{(1)}$ in DPD 1. The open stub $M_1^{(2)}$ is $\lambda/4$ at f_2. In other words, Point B_2 is a short circuit at f_2. Therefore, the input impedance $Z_{in1}^{(2)}|_{f=f_2} = \infty$ can be reached by designing the length of matching line $X_{T1}^{(2)}$ of Z_0 to equal $\lambda/4$ at f_2. On the basis of this design, the loading effect from the low-band circuit to the high-band circuit can be ignored. $M_2^{(2)}$ can help $M_1^{(2)}$ realize a microstrip form, which is similar to that of $M_4^{(1)}$ achieved with $M_3^{(1)}$ in DPD 1. Using a similar design, the loading effect from the high-band circuit to the low-band circuit can also be avoided by designing the length of matching line $X_{T2}^{(2)}$ of Z_0 to be equal to $\lambda/4$ at f_1, wherein the design of open stubs $M_7^{(2)}$ and $M_8^{(2)}$ is similar to that of stubs $M_{11}^{(1)}$ and $M_{12}^{(1)}$ in DPD 1. Moreover, each of stubs $M_5^{(2)}$, $M_6^{(2)}$, $M_{11}^{(2)}$, and $M_{12}^{(2)}$ is used to realize the capacitances C_g in Fig. 6.

The two band center frequencies of DPD 2 are $f_1 = 1.8$ GHz and $f_2 = 2.4$ GHz. The design parameters of DPD 2 are $R_1^{(2)} = 100\ \Omega$, $\theta_{M1}^{(2)}|_{f=f_1} = 67.5°$ or $\theta_{M1}^{(2)}|_{f=f_2} = 90°$, $\theta_{M2}^{(2)}|_{f=f_1} = 120°$ or $\theta_{M2}^{(2)} = 90°$at $f_{TZ1}^{(2)} = 1.35$ GHz, $\theta_{M3}^{(2)}|_{f=f_1} = \theta_{M4}^{(2)}|_{f=f_1} = 51.77°$, $\theta_{M5}^{(2)}|_{f=f_1} = \theta_{M6}^{(2)}|_{f=f_1} = 36°$, $Z_{M1}^{(2)} = 57.14\ \Omega$, $Z_{M2}^{(2)} = 70\ \Omega$, $Z_{M3}^{(2)} = Z_{M4}^{(2)} = 90\ \Omega$, $Z_{M5}^{(2)} = Z_{M6}^{(2)} = 83\ \Omega$, $R_2^{(2)} = 100\ \Omega$, $\theta_{M7}^{(3)}|_{f=f_2} = 120°$ or $\theta_{M7}^{(2)}|_{f=f_1} = 90°$, $\theta_{M8}^{(2)}|_{f=f_2} = 67.5°$ or $\theta_{M8}^{(2)} = 90°$ at $f_{TZ2}^{(2)} = 3.2$ GHz, $\theta_{M9}^{(2)}|_{f=f_2} = \theta_{M10}^{(2)}|_{f=f_2} = 51.77°$, $\theta_{M11}^{(2)}|_{f=f_2} = \theta_{M12}^{(2)}|_{f=f_2} = 36°$, $Z_{M7}^{(2)} = 70\ \Omega$, $Z_{M8}^{(2)} = 57.14\ \Omega$, $Z_{M9}^{(2)} = Z_{M10}^{(2)} = 90\ \Omega$, and $Z_{M11}^{(2)} = Z_{M12}^{(2)} = 83\ \Omega$, where $\theta_{Mi}^{(2)}$ and $Z_{Mi}^{(2)}$ represent the electrical length and characteristic impedance of $M_i^{(2)}(i = 1$ to $12)$, respectively.

Fig. 8 illustrates the circuit layout and photograph of DPD 2, wherein chip resistors are used to implement $R_1^{(2)}$ and $R_2^{(2)}$. Fig. 9 presents the simulated and measured frequency results of DPD 2. The measured minimal insertion loss ($-20\log|S_{21}|$) of the low-band divider was approximately 3.45 dB at 1.78 GHz. The measured minimal insertion loss ($-20\log|S_{41}|$) of the high-band divider was approximately 3.77 dB at 2.35 GHz. The measured value of $|S_{42}|$ was less than -18.2 dB between two operating bands. The measured maximal isolations -20log|S_{32}| and -20log|S_{54}| of the low-band and high-band dividers were approximately 28 dB at 1.81 GHz and 35 dB at 2.4 GHz, respectively. The measured magnitude and phase imbalances of the low-band divider operating band were approximately 0.2–0.43 dB and 1.42°–2.5°, respectively. The measured magnitude and phase imbalances of the high-band divider operating band were approximately 0.28–0.432 dB and 0.04°–0.854°, respectively. For $|S_{42}|$, four transmission zeros were measured at approximately 1.331 GHz, 1.785 GHz, 2.397 GHz, and 3.197 GHz approaching specifications of $f_{TZ1}^{(2)}$, f_1, f_2, and $f_{TZ2}^{(2)}$, respectively; these are contributed by stubs $M_2^{(2)}$, $M_7^{(2)}$, $M_1^{(2)}$, and $M_8^{(2)}$, respectively. For $|S_{21}|$, two transmission zeros were measured at approximately 1.331 GHz and 2.4 GHz approaching specifications of $f_{TZ1}^{(2)}$ and f_2, respectively; these are contributed by $M_2^{(2)}$ and $M_1^{(3)}$, respectively. For $|S_{41}|$, two transmission zeros were measured at approximately 1.785 GHz and 3.197 GHz approaching specifications of f_1 and $f_{TZ2}^{(2)}$, respectively; these are contributed by stubs $M_7^{(2)}$ and $M_8^{(2)}$, respectively. Comparing DPD 1 with DPD 2, low/high-band dividers are observed to have similar bandpass filtering and transmission zero responses. However, the matching

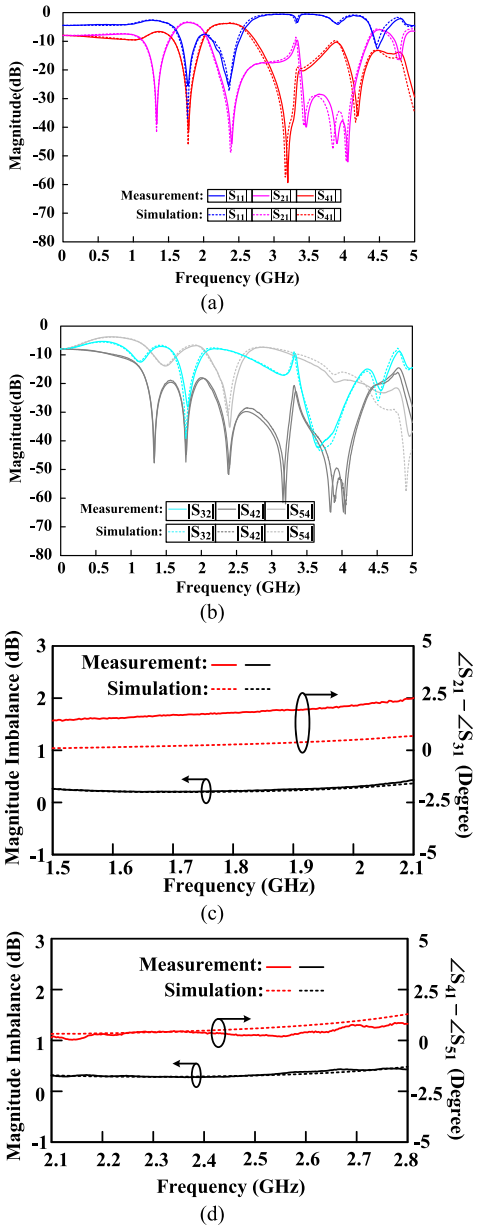

FIGURE 9. Measured and simulated responses of DPD 2. (a) $|S_{11}|$, $|S_{21}|$, and $|S_{41}|$. (b) $|S_{32}|$, $|S_{42}|$, and $|S_{54}|$. (c) Phase and magnitude imbalances of $|S_{21}|$ and $|S_{31}|$. (d) Phase and magnitude imbalances of $|S_{41}|$ and $|S_{51}|$.

length designs of lines $X_{T1}^{(1)}$ and $X_{T2}^{(1)}$ in DPD 1 and lines $X_{T1}^{(2)}$ and $X_{T2}^{(2)}$ in DPD 2 are somewhat different, wherein the length of $X_{T1}^{(1)}/X_{T2}^{(1)}$ is varied by $Z_{in1}^{(1)'}\big|_{f=f_2}/Z_{in2}^{(1)'}\big|_{f=f_1}$ and that of $X_{T1}^{(2)}/X_{T2}^{(2)}$ is fixed at $\lambda/4$ of f_2/f_1.

IV. DESIGN OF DPD 3

From (3), a high characteristic impedance (Z_g) is required to achieve a short length (small size) of the series transmission line section S_g in Fig. 5. However, this could be a challenge in microstrip form. This problem can be overcome by replacing the π-shaped lumped impedance transformers in Fig. 10(a) and Fig. 10(b) [28] with 90° and −90°

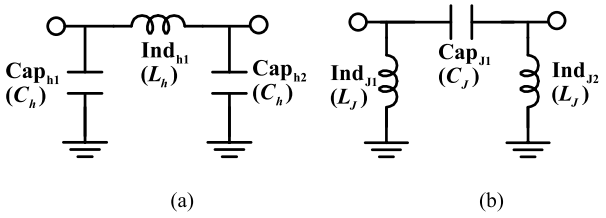

FIGURE 10. (a) π-shaped impedance transformer with a series inductor and two shunt capacitors. (b) π-shaped impedance transformer with a series capacitor and two shunt inductors.

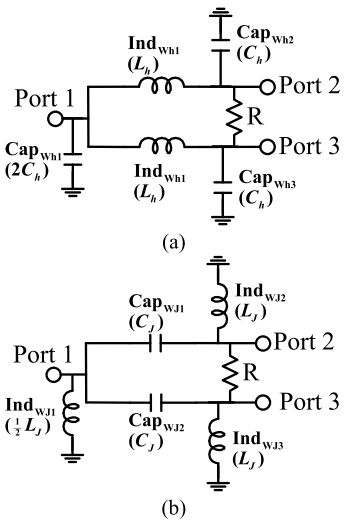

FIGURE 11. (a) Modified WPD with a series inductor and shunt capacitors in each transmission path. (b) A modified WPD with a series capacitor and shunt inductors in each transmission path.

transformers, respectively, wherein inductance L_h and capacitance C_J are designed by chip inductor and capacitor to avoid the difficult microstrip form realization of high characteristic impedance for S_g. In WPD, the 90° transformers can be replaced by −90° impedance transformers. The design equations between 90° and −90° impedance transformers of WPD and the π-shaped impedance transformer in Fig. 10 can be written as

$$Z_1 = X_h \tag{5}$$

$$0 = 1 - B_h X_h \tag{6}$$

$$0 = 1 - \frac{1}{B_J X_J} \tag{7}$$

$$Z_1 = \frac{1}{B_J} \tag{8}$$

where X_h/X_J denotes the reactance of inductance L_h/L_J, and B_h/B_J denotes the susceptance of capacitance C_h/C_J. The modified WPDs in Fig. 11(a) and Fig. 11(b) can be obtained using the two π-shaped circuits in Fig. 10(a) and Fig. 10(b) to design their impedance transformers, respectively, where Cap_{Wh1}/Ind_{WJ1} is equivalent to the value of capacitance $2C_h$/inductance $\frac{1}{2}L_J$ in parallel. Fig. 12 illustrates the proposed DPD 3 ideal equivalent circuit comprising a low-band divider, a high-band divider, and two matching lines

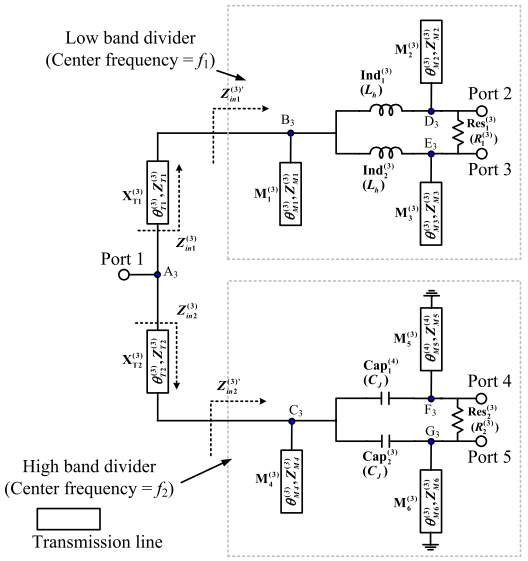

FIGURE 12. Proposed DPD 3 equivalent circuit.

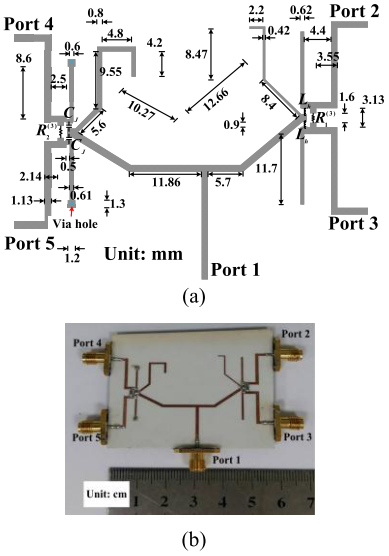

FIGURE 13. Proposed DPD 3 (a) layout and (b) photograph.

($X_{T1}^{(3)}$ and $X_{T2}^{(3)}$) with Z_0 characteristic impedance, wherein the low- and high-band dividers use the modified WPDs, as shown in Fig. 11; the resistance $R_1^{(3)}$ or $R_2^{(3)}$ is $2Z_0$. The center frequencies of the low-band and high-band dividers are $f_1 = 1.8$ GHz and $f_2 = 2.4$ GHz, respectively. The f_1 susceptance of open stub $M_2^{(3)}/M_3^{(3)}$ and the f_2 reactance of short stub $M_5^{(3)}/M_6^{(3)}$ equal f_1 susceptance of C_h and f_2 reactance of L_J, respectively. The susceptance of open stub $M_1^{(3)}$ equals that of $2C_h$ in Fig. 10 and the length of $M_1^{(3)}$ is $\lambda/4$ at f_2. In other words, Point B_3 is a short circuit at f_2. Therefore, the input impedance $Z_{in1}^{(3)}$ at f_2 can reach infinity by designing the length of matching line $X_{T1}^{(3)}$ of Z_0 to equal $\lambda/4$ at f_2. On the basis of this design, the loading effect from the low-band circuit to the high-band circuit can be ignored. Using a similar design, the loading effect from the high-band circuit to the low-band circuit can also be avoided by designing the length of matching line $X_{T2}^{(3)}$ of Z_0 to equal $\lambda/4$ at f_1. Therefore, the input impedance $Z_{in2}^{(3)}$ at f_1 can reach infinity.

The design parameters of DPD 3 are $R_1^{(3)} = 100\ \Omega$, $\theta_{M1}^{(4)}|_{f=f_1} = 67.5°$ or $\theta_{M1}^{(3)}|_{f=f_2} = 90°$, $\theta_{M2}^{(3)} = \theta_{M3}^{(3)} = 45°$ at $f_1 = 1.8$ GHz or 90° at $f_{TZ1}^{(3)} = 3.6$ GHz, $Z_{M1}^{(3)} = 85.34\ \Omega$, $Z_{M2}^{(3)} = Z_{M3}^{(3)} = 70.7\ \Omega$, $L_h = 6.25125$ nH, $R_2^{(3)} = 100\ \Omega$, $\theta_{M4}^{(3)}|_{f=f_1} = 90°$ or $\theta_{M4}^{(3)}|_{f=f_2} = 120°$, $\theta_{M5}^{(3)}|_{f=f_2} = \theta_{M6}^{(3)}|_{f=f_2} = 45°$, $Z_{M4}^{(3)} = 61.22\ \Omega$, $Z_{M5}^{(3)} = Z_{M6}^{(3)} = 70.7\ \Omega$, and $C_J = 0.938$ pF, where $\theta_{Mi}^{(3)}$ and $Z_{Mi}^{(3)}$ represent the electrical length and characteristic impedance of $M_i^{(3)}(i = 1$ to 6), respectively.

Fig. 13 illustrates the circuit layout and photograph of DPD 3, wherein a chip resistor, capacitor, and inductor are used to implement lumped elements. Fig. 14 presents the simulated and measured frequency results of DPD 3. In the operating band, the measured minimal insertion loss ($-20\log|S_{21}|$) of the low-band divider was approximately 3.5 dB at 1.75 GHz; the measured minimal insertion loss ($-20\log|S_{41}|$) of the high-band divider was approximately 3.74 dB at 2.4 GHz. The measured value of $|S_{42}|$ was less than -18.7 dB between two operating bands. The measured maximal isolations $-20\log|S_{32}|$ and $-20\log|S_{54}|$ of the low-band and high-band dividers were approximately 30 dB at 1.738 GHz and 32 dB at 2.28 GHz, respectively. The measured magnitude and phase imbalances of the low-band divider operating band were approximately 0.12–1.498 dB and 1.07°–7.74°, respectively. The measured magnitude and phase imbalances of the high-band divider operating band were approximately 0–1.197 dB and 0.06°–2.74°, respectively. For $|S_{42}|$, three transmission zeros were measured at approximately 1.866 GHz, 2.478 GHz, and 3.5 GHz approaching specifications of f_1, f_2, and $f_{TZ1}^{(3)}$, respectively; these are contributed by stubs $M_4^{(3)}$, $M_1^{(3)}$, and $M_2^{(3)}$, respectively. For $|S_{21}|$, transmission zeros were measured at approximately 2.478 GHz and 3.506 GHz approaching specifications of f_2 and $f_{TZ1}^{(3)}$, respectively; these are contributed by $M_1^{(3)}$ and $M_2^{(3)}$, respectively. For $|S_{41}|$, the transmission zero was measured at approximately 1.866 GHz approaching specification of f_1, which is contributed by stub $M_4^{(3)}$.

Although DPD 2 and DPD 3 use the π-shaped equivalent transformer to design the low/high-band dividers, the primary difference is only one $\lambda/4$ open stub near each divider input of DPD 3; however, in this paper, two stubs exist near each divider input of DPD 2. From (3) and (4) of DPD 2, the following equation can be obtained:

$$B_g = \frac{\cos\theta_g}{Z_1}. \tag{9}$$

From (5) and (6) of DPD 3, the following equation can be obtained:

$$B_h = \frac{1}{Z_1}. \tag{10}$$

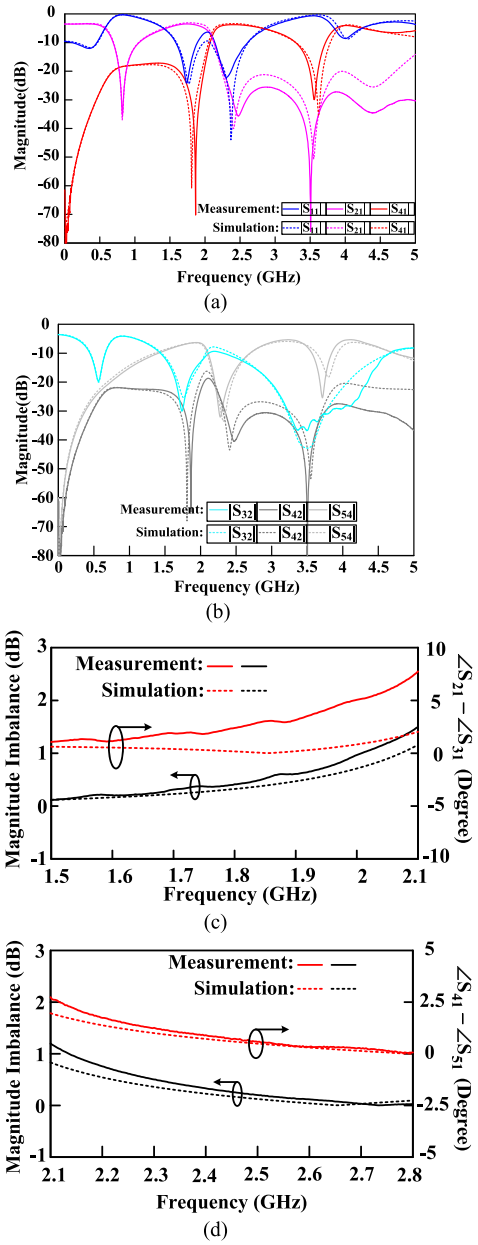

FIGURE 14. Measured and simulated responses of DPD 4. (a) $|S_{11}|$, $|S_{21}|$, and $|S_{41}|$. (b) $|S_{32}|$, $|S_{42}|$, and $|S_{54}|$. (c) Phase and magnitude imbalances of $|S_{21}|$ and $|S_{31}|$. (d) Phase and magnitude imbalances of $|S_{41}|$ and $|S_{51}|$.

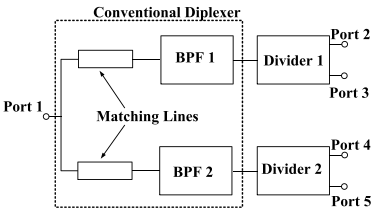

FIGURE 15. Equivalent circuit model of a conventional diplexer cascaded to different band dividers.

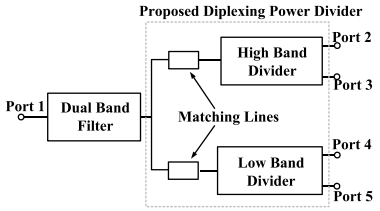

FIGURE 16. Equivalent circuit model a dual-band filter cascaded to the proposed DPD.

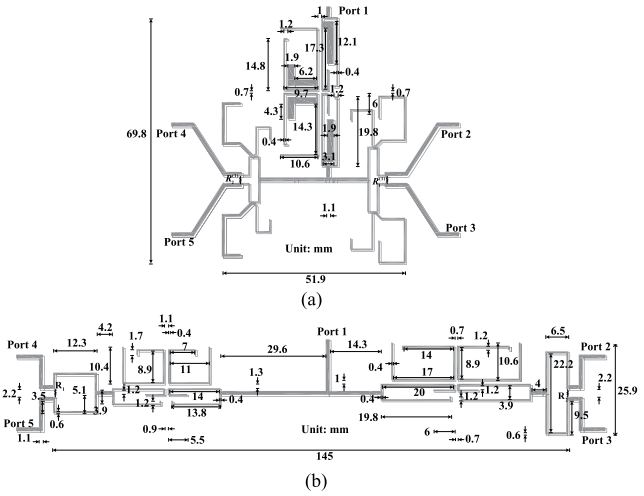

FIGURE 17. (a) A dual-band filter cascaded to the proposed DPD 1. (b) Two different band WPDs cascaded to the output ports of a conventional diplexer.

From (9) and (10), $B_h > B_g$ when $0° < \theta_g < 90°$. For example, $\theta_g = \theta_{M3}^{(2)} = 51.77°$ is designed in the low-band divider of DPD 2 and $Z_1 = 70.7\ \Omega$ is designed in that of DPD 2 or DPD 3. $B_h = 1.62B_g$ is calculated. Under this condition, compared with B_g, reasonable characteristic impedance can be realized to fit the larger B_h value by using only one microstrip open stub at $\lambda/4$ of f_2 in DPD 3. However, DPD 2 needs an assistant stub $M_2^{(2)}$ to realize reasonable characteristic impedance $\lambda/4$ for $M_1^{(2)}$ stub under small B_g.

In a high-band channel, DPD 2 or DPD 3 needs a 90° open stub $M_7^{(2)}$ or $M_4^{(3)}$ at f_1. In other words, the electrical length of $M_7^{(2)}$ or $M_4^{(3)}$ is larger than 90° at f_2 because $f_1 < f_2$. For example, in this study, $f_1/f_2 = 3/4$ and the electrical length of $M_7^{(2)}$ or $M_4^{(3)}$ is 120° at f_2, that is, $M_7^{(2)}$ or $M_4^{(3)}$ is equivalent to an inductance at f_2. However, near the input of DPD 2, the high-band divider needs an equivalent shunt capacitance. At f_2, the inductance (using a single stub $M_7^{(2)}$) can be turned into the required design capacitance by adding the assistant shunt stub $M_8^{(2)}$. In the high-band divider, DPD 3 can use only one $\lambda/4$ of f_1 $M_4^{(3)}$ to meet the required $\frac{1}{2}X_J$ because the input of the high-band divider needs an equivalent shunt inductance. Although DPD 3 has advantages of small size contributed by chip capacitors and inductors and only one stub near each band divider, the additional chip capacitors and inductors result in an increase in the lump element cost and additional unwanted parasitic effect.

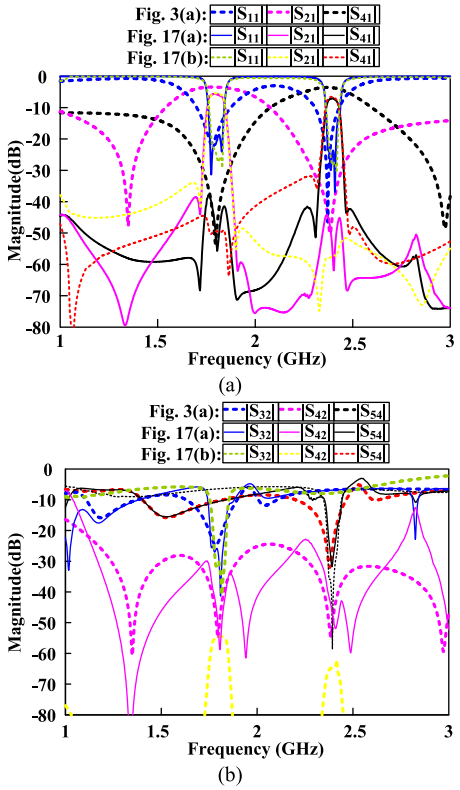

FIGURE 18. Simulated comparisons of Fig. 3(a), Fig. 17(a), and Fig. 17(b). (a) $|S_{11}|$, $|S_{21}|$, and $|S_{41}|$. (b) $|S_{32}|$, $|S_{42}|$, and $|S_{54}|$.

V. DISCUSSION

As shown in Fig 15, antenna gains for different frequency bands can be increased by cascading different band power dividers (Divider 1 and Divider 2) to a conventional diplexer in the RF front-end circuit system, wherein different band antennas are connected at Ports 2–3 and Ports 4–5, respectively. The diplexer comprises two bandpass filters with different frequency bands (BPF 1 and BPF 2) and two 50-Ω matching lines. Fig. 16 illustrates a dual-band filter cascaded to the proposed DPD structure, which has a similar function of Fig. 15 for increasing the gains of antennae with different frequency bands. This paper presents three types of DPD structures (DPD 1, DPD 2, and DPD 3) for increasing the antenna gains in 1.8 GHz (LTE) and 2.4 GHz (Wi-Fi) band systems. In particular, both DPD 1 and DPD 2 have a bandpass response with transmission zeros at the lower and upper stopbands for each transmission band; that is, DPD 1 or DPD 2 has satisfactory selectivity in each transmission path, despite not requiring an additional filter. Fig. 17(a) shows a dual-band filter [25] cascaded to input port of Fig. 3(a) (DPD 1), wherein stub-loaded resonators [26] are used to the filter design. In Fig. 17(b), two WPDs are connected to a conventional diplexer, wherein the diplexer uses two 50-Ω lines to design the junction matching of two different band cross-coupled filters [29]; 100-Ω isolation resistors R_1 and R_2 are used to the different band WPDs. In Fig. 17, the two operating frequencies f_1 and f_2 are approximately 1.8 GHz and 2.4 GHz, respectively 3-dB fractional bandwidths of the high- and low-band are approximately 4.4 % and 2.7%. Fig. 18 shows the simulated comparisons of Fig. 3(a), Fig. 17(a), and Fig. 17(b). For $20\log|S_{21}|$, the minimal values are 3.4 dB, 5.6 dB, and 5.4 dB, respectively. For $20\log|S_{41}|$, the minimal values are 3.5 dB, 7 dB, and 6.6 dB, respectively. In Fig. 17(a), the dual-band filter contributes approximately 2.2 dB and 3.5 dB transmission losses for low- and high-band channels, respectively. In general, bandpass filter has serious loss issue when high selectivity response and narrow bandwidth are needed. Therefore, the presented DPD circuits have the flexibility to add extra dual-band bandpass filter depending on low loss or high selectivity requirement after finishing the designs of DPDs. However, by cascading two different band conventional WPDs to output ports of a conventional diplexer, the two filters can not remove form the dilplexer because each channel 50-Ω matching line is difficult to achieve the required open condition under avoiding the filters. In other words, input impedance of each WPD without filter can not approach outside circle of Smith chart near the other band. Therefore, 50-Ω matching line can not bring it to approach the required open condition near the other band.

VI. CONCLUSION

In this paper, three new microstrip DPDs using integrated matching circuits in dividers were proposed. In the proposed DPDs, the integrated matching circuits ensure that each band divider with pure imaginary input impedance or a short circuit can achieve the required open condition by adding a 50-Ω transmission line of appropriate length or a λ/4 transmission line before the divider. With the proposed matching designs, each DPD can easily decide each band channel response and may facilitate the design process. Moreover, all the proposed DPDs designs were carefully verified.

REFERENCES

[1] B. Strassner and K. Chang, "Wide-band low-loss high-isolation microstrip periodic-stub diplexer for multiple-frequency applications," *IEEE Trans. Microw. Theory Techn.*, vol. 49, no. 10, pp. 1818–1820, Oct. 2001.

[2] C.-M. Tsai, S.-Y. Lee, C.-C. Chuang, and C.-C. Tsai, "A folded coupled-line structure and its application to filter and diplexer design," in *IEEE MTT-S Int. Microw. Symp. Dig.*, Jun. 2002, pp. 1927–1930.

[3] S. Srisathit, S. Patisang, R. Phromloungsri, S. Bunnjaweht, S. Kosulvit, and M. Chongcheawchamnan, "High isolation and compact size microstrip hairpin diplexer," *IEEE Microw. Wireless Compon. Lett.*, vol. 15, no. 2, pp. 101–103, Feb. 2005.

[4] C.-W. Tang and S.-F. You, "Design methodologies of LTCC bandpass filters, diplexer, and triplexer with transmission zeros," *IEEE Trans. Microw. Theory Techn.*, vol. 54, no. 2, pp. 717–723, Feb. 2006.

[5] C.-F. Chen, T. Huang, C.-P. Chou, and R. Wu, "Microstrip diplexers design with common resonator sections for compact size, but high isolation," *IEEE Trans. Microw. Theory Techn.*, vol. 54, no. 5, pp. 1945–1952, May 2006.

[6] M. H. Weng, C. Y. Hung, and Y. K. Su, "A hairpin line diplexer for direct sequence ultra-wideband wireless communications," *IEEE Microw. Wireless Compon. Lett.*, vol. 17, no. 7, pp. 519–521, Jul. 2007.

[7] T. Yang, P.-L. Chi, and T. Itoh, "High isolation and compact diplexer using the hybrid resonators," *IEEE Microw. Wireless Compon. Lett.*, vol. 20, no. 10, pp. 551–553, Oct. 2010.

[8] T. Yang, P.-L. Chi, and T. Itoh, "Compact quarter-wave resonator and its applications to miniaturized diplexer and triplexer," *IEEE Trans. Microw. Theory Techn.*, vol. 59, no. 2, pp. 260–269, Feb. 2011.
[9] M.-L. Chuang and M.-T. Wu, "Microstrip diplexer design using common T-shaped resonator," *IEEE Microw. Wireless Compon. Lett.*, vol. 21, no. 11, pp. 583–585, Nov. 2011.
[10] J. Y. Zou, C. H. Wu, and T. G. Ma, "Miniaturized diplexer using synthesized microstrip lines with series LC tanks," *IEEE Microw. Wireless Compon. Lett.*, vol. 22, no. 7, pp. 354–356, Jul. 2012.
[11] P.-H. Deng and J.-T. Tsai, "Design of microstrip lowpass-bandpass diplexer," *IEEE Microw. Wireless Compon. Lett.*, vol. 23, no. 7, pp. 332–334, Jul. 2013.
[12] P.-H. Deng, R.-C. Liu, W.-D. Lin, and W. Lo, "Design of a microstrip lowpass-bandpass diplexer using direct-feed coupled-resonator filter," *IEEE Microw. Wireless Compon. Lett.*, vol. 27, no. 3, pp. 254–256, Mar. 2017.
[13] E. J. Wilkinson, "An N-way hybrid power divider," *IRE Trans. Microw. Theory Techn.*, vol. MTT-8, no. 1, pp. 116–118, Jan. 1960.
[14] L.-H. Lu, P. Bhattacharya, L. P. B. Katehi, and G. E. Ponchak, "X-band and K-band lumped Wilkinson power dividers with a micromachined technology," in *IEEE MTT-S Int. Microw. Symp. Dig.*, Jun. 2000, pp. 287–290.
[15] M. C. Scardelletti, G. E. Ponchak, and T. M. Weller, "Miniaturized Wilkinson power dividers utilizing capacitive loading," *IEEE Microw. Wireless Compon. Lett.*, vol. 12, no. 1, pp. 6–8, Jan. 2002.
[16] K.-H. Yi and B. Kang, "Modified Wilkinson power divider for nth harmonic suppression," *IEEE Microw. Wireless Compon. Lett.*, vol. 13, no. 5, pp. 178–180, May 2003.
[17] W. H. Tu, "Compact Wilkinson power divider with harmonic suppression," *Microw. Opt. Tech. Lett.*, vol. 49, no. 11, pp. 2825–2827, Nov. 2007.
[18] Y. L. Wu, H. Zhou, Y. X. Zhang, and Y. A. Liu, "An unequal Wilkinson power divider for a frequency and its first harmonic," *IEEE Microw. Wireless Compon. Lett.*, vol. 18, no. 11, pp. 737–739, Nov. 2008.
[19] J. Wang, J. Ni, Y.-X. Guo, and D. Fang, "Miniaturized microstrip Wilkinson power divider with harmonic suppression," *IEEE Microw. Wireless Compon. Lett.*, vol. 19, no. 7, pp. 440–442, Jul. 2009.
[20] S.-H. Ahn, J. W. Lee, C. S. Cho, and T. K. Lee, "A dual-band unequal Wilkinson power divider with arbitrary frequency ratios," *IEEE Microw. Wireless Compon. Lett.*, vol. 19, no. 12, pp. 783–785, Dec. 2009.
[21] Q.-X. Chu, F. Lin, Z. Lin, and Z. Gong, "Novel design method of triband power divider," *IEEE Trans. Microw. Theory Techn.*, vol. 59, no. 9, pp. 2221–2226, Sep. 2011.
[22] P. H. Deng and L. C. Dai, "Unequal Wilkinson power dividers with favorable selectivity and high-isolation using coupled-line filter transformers," *IEEE Trans. Microw. Theory Techn.*, vol. 60, no. 6, pp. 1520–1529, Jun. 2012.
[23] C.-F. Chen, T.-Y. Huang, T.-M. Shen, and R.-B. Wu, "Design of miniaturized filtering power dividers for system-in-a-package," *IEEE Compon., Packag., Manuf. Technol.*, vol. 3, no. 10, pp. 1663–1672, Oct. 2013.
[24] P.-H. Deng and Y.-T. Chen, "New Wilkinson power dividers and their integration applications to four-way and filtering dividers," *IEEE Compon., Packag., Manuf. Technol.*, vol. 4, no. 11, pp. 1828–1837, Nov. 2014.
[25] J. T. Kuo and H.-S. Cheng, "Design of quasi-elliptic function filters with a dual-passband response," *IEEE Microw. Wireless Compon. Lett.*, vol. 14, no. 10, pp. 472–474, Oct. 2004.
[26] X. Y. Zhang, J.-X. Chen, Q. Xue, and S.-M. Li, "Dual-band bandpass filters using stub-loaded resonators," *IEEE Microw Wireless Compon. Lett.*, vol. 17, no. 8, pp. 583–585, Aug. 2007.
[27] P.-H. Deng, J.-T. Tsai, and R.-C. Liu, "Design of a switchable microstrip dual-band lowpass-bandpass filter," *IEEE Microw. Wireless Compon. Lett.*, vol. 24, no. 9, pp. 599–601, Sep. 2014.
[28] T.-M. Shen, C.-R. Chen, T.-Y. Huang, and R.-B. Wu, "Design of lumped rat-race coupler in multilayer LTCC," in *Proc. Asia–Pacific Microw. Conf.*, Dec. 2009, pp. 2120–2123.
[29] J.-S. Hong and M. J. Lancaster, "Cross-coupled microstrip hairpin-resonator filters," *IEEE Trans. Microw. Theory Techn.*, vol. 46, no. 1, pp. 118–122, Jan. 1998.

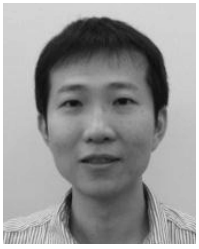

PU-HUA DENG was born in Kaohsiung, Taiwan, in 1978. He received the B.Sc. degree in electrical engineering from National Sun Yet-Sen University, Kaohsiung, in 2002, and the M.Sc. and Ph.D. degrees in communication engineering from National Taiwan University, Taipei, Taiwan, in 2004 and 2006, respectively. In 2006, he joined ZyXEL Communication Corporation, Hsinchu, Taiwan, where he was a RF Engineer. In 2007, he joined NXP Semiconductors Company, Kaohsiung, where he was an Advanced RF Testing Engineer. From 2008 to 2009, he joined the faculty of the Department of Electrical Engineering, National University of Tainan, Tainan, Taiwan, as an Assistant Professor. Since 2009, he has been a Faculty Member with the Department of Electrical Engineering, National University of Kaohsiung, Kaohsiung, where he is currently a Professor. His research interests include the design and analysis of microwave planar circuits.

WEI LO received the M.Sc. degree in electrical engineering from the National University of Tainan, Tainan, Taiwan, in 2016. His research interests include microwave filters and multiplexers.

BO-LIN CHE was born in Tainan, Taiwan, in 1991. He received the B.Sc. degree in electrical engineering from Shu-Te University, Kaohsiung, Taiwan, in 2013, and the M.Sc. degree in electrical engineering from the National University of Kaohsiung, Kaohsiung, in 2015. His research interests include microwave circuits.

CHEN-HSIANG LIN received the B.Sc. degree from the Department of Electronic Communication Engineering, National Kaohsiung Marine University, Kaohsiung, Taiwan, in 2015, and the degree in electrical engineering from the National University of Kaohsiung, Kaohsiung. His research interests include microwave filters and multiplexers.